Supplement of Hydrol. Earth Syst. Sci., 29, 1429–1447, 2025
https://doi.org/10.5194/hess-29-1429-2025-supplement

Hydrology and Earth System Sciences
Open Access
EGU

Supplement of

Exploring the value of seasonal flow forecasts for drought management in South Korea

Yongshin Lee et al.

Correspondence to: Yongshin Lee (yongshin.lee@bristol.ac.uk)

S1. Pareto-front normalisation

Given the dimensional disparity between the two objectives (SSD, SVD), transforming the Pareto front can offer advantages, and normalisation is considered the most robust approach (Marler and Arora, 2004). Therefore, before applying each MCDM method, we normalized the Pareto-front. Among the numerous normalisation methods, we applied the widely used Min-max method. This method holds advantages in preserving the relationships among the original data (Han et al., 2012) and has demonstrated good performance, particularly in the SAW method (Mathew et al., 2017; Vafaei et al., 2022). Although this method is known for its sensitivity to outliers in extreme data (Han et al., 2012), the Pareto front generated from Eqs. 5 and 6 consists of continuous points without outliers. It performs a linear transformation on the original data and confines each objective in the range 0 to 1 as described by the following equation:

$$x_{normalised} = \frac{x - \min(x)}{\max(x) - \min(x)} \quad \text{(S1)}$$

where $x, \min(x)$ and $\max(x)$ represent a point, minimum and maximum point within the Pareto fronts, respectively.

S2. Multi-Criteria Decision-Making method

The SAW method, which is one of frequently employed methods in decision-making (Arsyah et al., 2021), ranks the alternatives based on their weighted sum performance (Fishburn, 1967). Given our aim to minimize SSD and SVD, the selected compromise solution is the one with the smallest weighted sum, as expressed below:

$$Compromise\ solution_{SAW} = \min(w_{SSD} \times SSD_i + w_{SVD} \times SVD_i) \quad \text{(S2)}$$

where, w_{SSD} and w_{SVD} are the weights for supply and storage. SSD_i and SVD_i represent the normalized objectives at the *i*th point within the Pareto front (i = 1, … ,100). In this study, we consider the 'balanced' method where equal weights are assigned to each objective ($w_{SSD} = w_{SVD} = 0.5$), as well as the 'storage-prioritised' and 'supply-prioritised' methods, which prioritise storage ($w_{SSD} = 0.4$, $w_{SVD} = 0.6$) and supply ($w_{SSD} = 0.6$, $w_{SVD} = 0.4$), respectively.

The 'variable weighting' method, which uses again Eq. S2 but assigns different weights according to the storage volume at the time when the decision is taken. We applied this method in two ways: the 'simple selective' method, which adopts the same weights as in the SAW methods but varying them depending on storage status, and the 'multi-weight' method, which applies more detailed procedure to allocate weights based on storage status. In doing so, we analysed around 20 years of historical storage records to divide the storage into multiple ranges, then specified a method or weight for each range (see Figure S1).

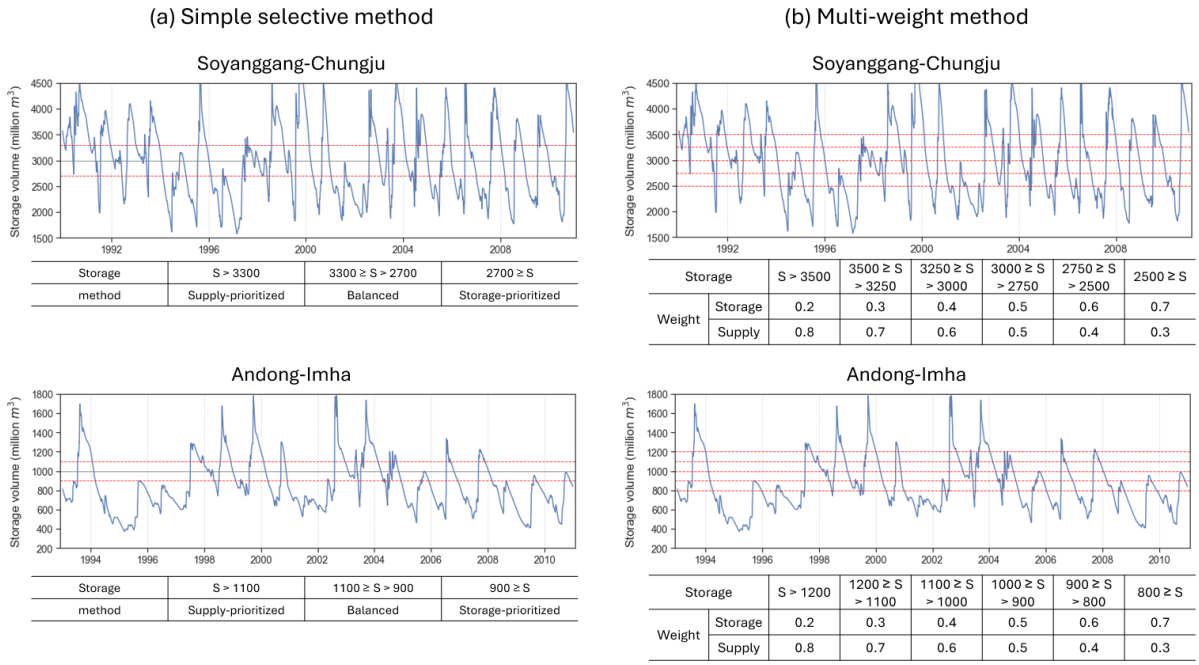

Storage	S > 3300	3300 ≥ S > 2700	2700 ≥ S
method	Supply-prioritized	Balanced	Storage-prioritized

Storage		S > 3500	3500 ≥ S > 3250	3250 ≥ S > 3000	3000 ≥ S > 2750	2750 ≥ S > 2500	2500 ≥ S
Weight	Storage	0.2	0.3	0.4	0.5	0.6	0.7
	Supply	0.8	0.7	0.6	0.5	0.4	0.3

Storage	S > 1100	1100 ≥ S > 900	900 ≥ S
method	Supply-prioritized	Balanced	Storage-prioritized

Storage		S > 1200	1200 ≥ S > 1100	1100 ≥ S > 1000	1000 ≥ S > 900	900 ≥ S > 800	800 ≥ S
Weight	Storage	0.2	0.3	0.4	0.5	0.6	0.7
	Supply	0.8	0.7	0.6	0.5	0.4	0.3

Figure S1: (a) Simple selective method: the storage ranges and applied SAW method in each range. (b) Multi-weight method: the storage ranges and applied weight in each range. The blue lines represent the daily reservoir operation records for Soyanggang-Chungju (top row) and Andong-Imha (bottom row) reservoir systems.

The reference point method identifies the compromise solution on a Pareto front by measuring the distance from a reference point. In this study, we applied three versions of this approach: 'utopian point', 'knee point', and 'TOPSIS' methods. Application examples of these methods are illustrated in Figure S2.

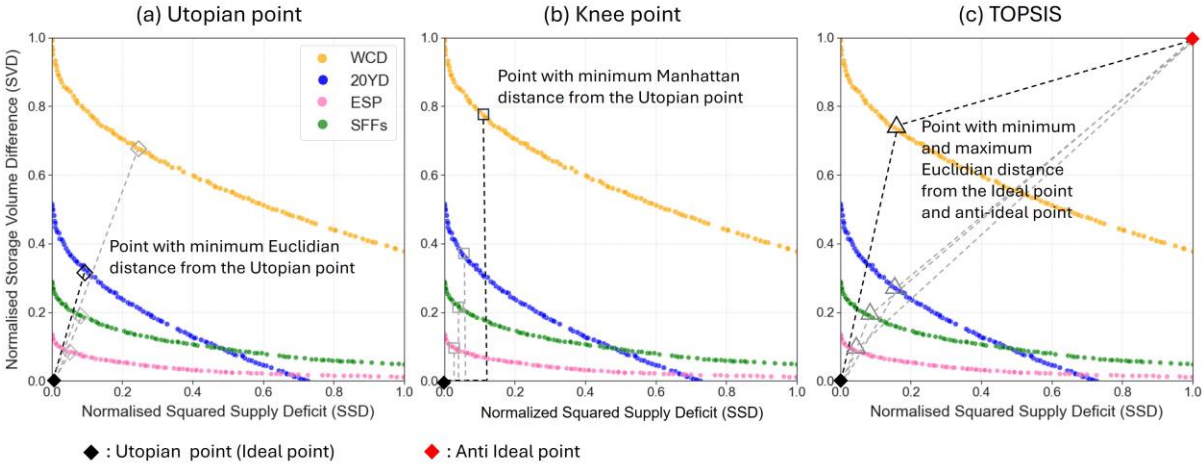

Figure S2: An example of the reference point method, including (a) Utopian Point, (b) Knee Point, and (c) TOPSIS method, generated for June 2014 with a 4-month lead time using different flow forecasts (WCD: yellow, 20YD: blue, ESP: pink, SFFs: green).

The utopian point method selects the solution on the Pareto front that minimizes the Euclidean distance from the utopian (or ideal) point, which represents the theoretical perfect solution (Lu et al., 2011). The knee point method selects the knee point, which is a point where the curvature of the Pareto front is maximum (Das, 1999). Among various methods for detecting the knee point, we adopted the approach based on Minimum Manhattan Distance from the utopian point (Chiu et al., 2016). This approach has been demonstrated to be both simple and robust in the literature (Li et al., 2020). Compromise solutions from these two methods are computed as:

$$Compromise\ solution_{Utopian} = \min\left(\sqrt{\left(SSD_i - SSD_{utopian}\right)^2 + \left(SVD_i - SVD_{utopian}\right)^2}\right) \quad \text{(S3)}$$

$$Compromise\ solution_{Knee} = \min(\left|SSD_i - SSD_{utopian}\right| + \left|SVD_i - SVD_{utopian}\right|) \quad \text{(S4)}$$

where $i = 1, \ldots, 100$ is the number of points (each corresponding to a Pareto-optimal release schedule) on the Pareto front. SSD_i and SVD_i denote a normalized point of each objective at the ith point (see Eqs. 5 and 6 in main manuscript). SSD_{utopia} and SVD_{utopia} are the utopian points of each objective, which are equal to [0, 0].

The TOPSIS method, developed by Hwang and Yoon (1981), is a widely chosen method for MCDM (Tzeng and Huang, 2011; Wang and Rangaiah, 2017) and is recommended by the United Nations Environmental Program (Chen, 2000; Zhu et al., 2015). It selects a point with the shortest Euclidian distance from the ideal point [0, 0] and the longest distance from the anti-ideal point [1, 1] as the compromise solution (Hwang and Yoon, 1981; Liu, 2009). This can be expressed as:

$$Distance_i^{ideal} = \sqrt{(SSD_i - SSD_{ideal})^2 + (SVD_i - SVD_{ideal})^2} \quad \text{(S5)}$$

$$Distance_i^{anti-ideal} = \sqrt{(SSD_{anti-ideal} - SSD_i)^2 + (SVD_{anti-ideal} - SVD_i)^2} \quad \text{(S6)}$$

$$CC_i = \frac{Distance_i^{anti-ideal}}{Distance_i^{ideal} + Distance_i^{anti-ideal}} \quad \text{(S7)}$$

where $Distance_i^{ideal}$ and $Distance_i^{anti-ideal}$ are the Euclidian distances from ideal and anti-ideal points to ith point and CC_i is the closeness coefficient of the ith point. Since a higher closeness coefficient indicates a better solution, the point with the highest CC_i is selected as the compromise solution.

S3. Supplementary figures

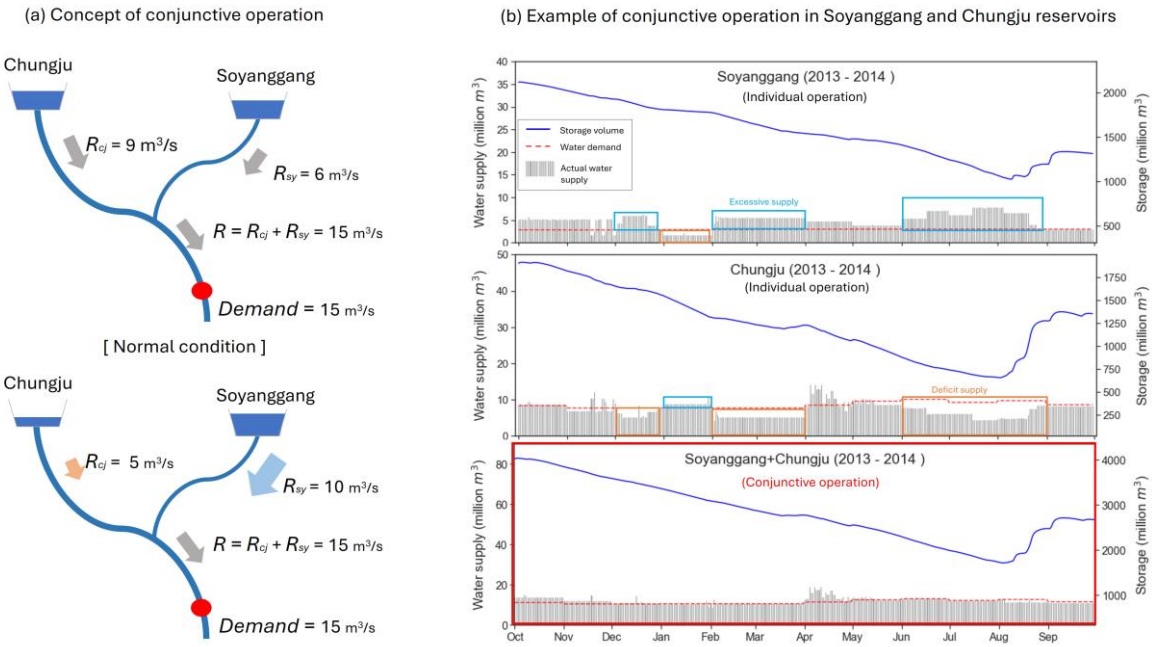

Figure S3: (a) Concept of conjunctive reservoir operations. (b) Daily reservoir operation records from October 2013 to September 2014 for Soyangang reservoir alone (first row), Chungju reservoir alone (second row) and their conjunctive operation (third row).

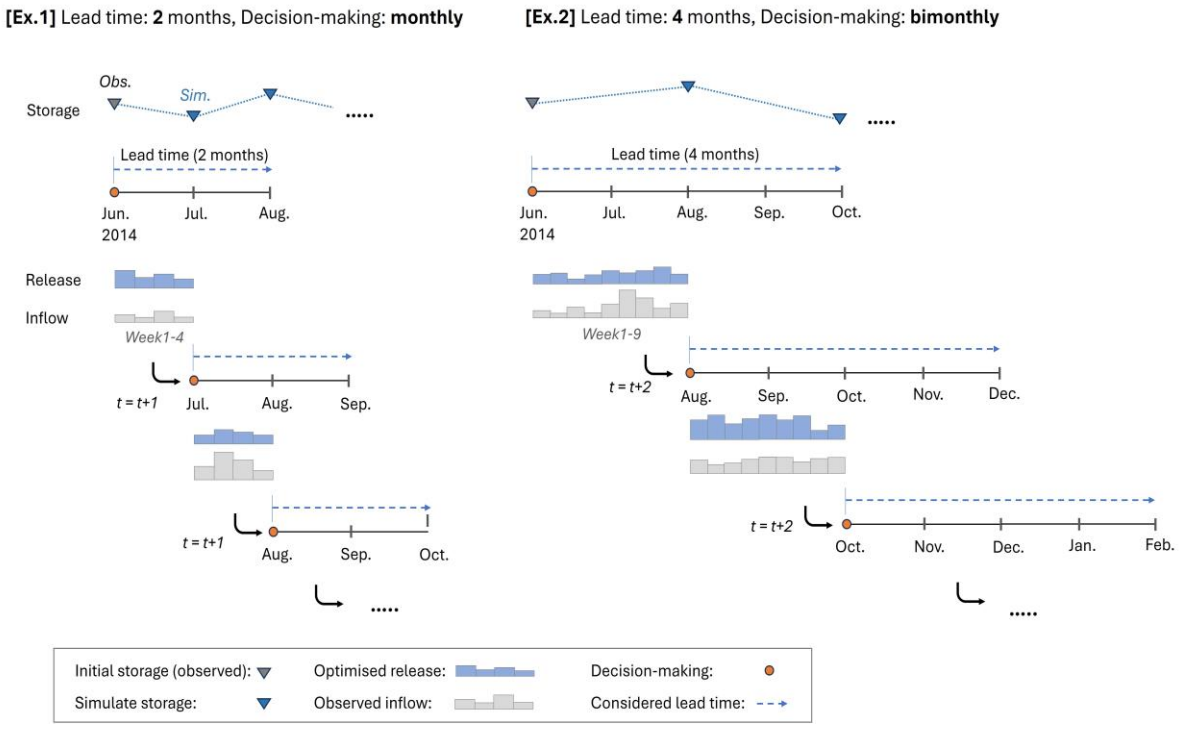

Figure S4: Conceptual examples of our continuous reservoir simulation with different experimental choices.

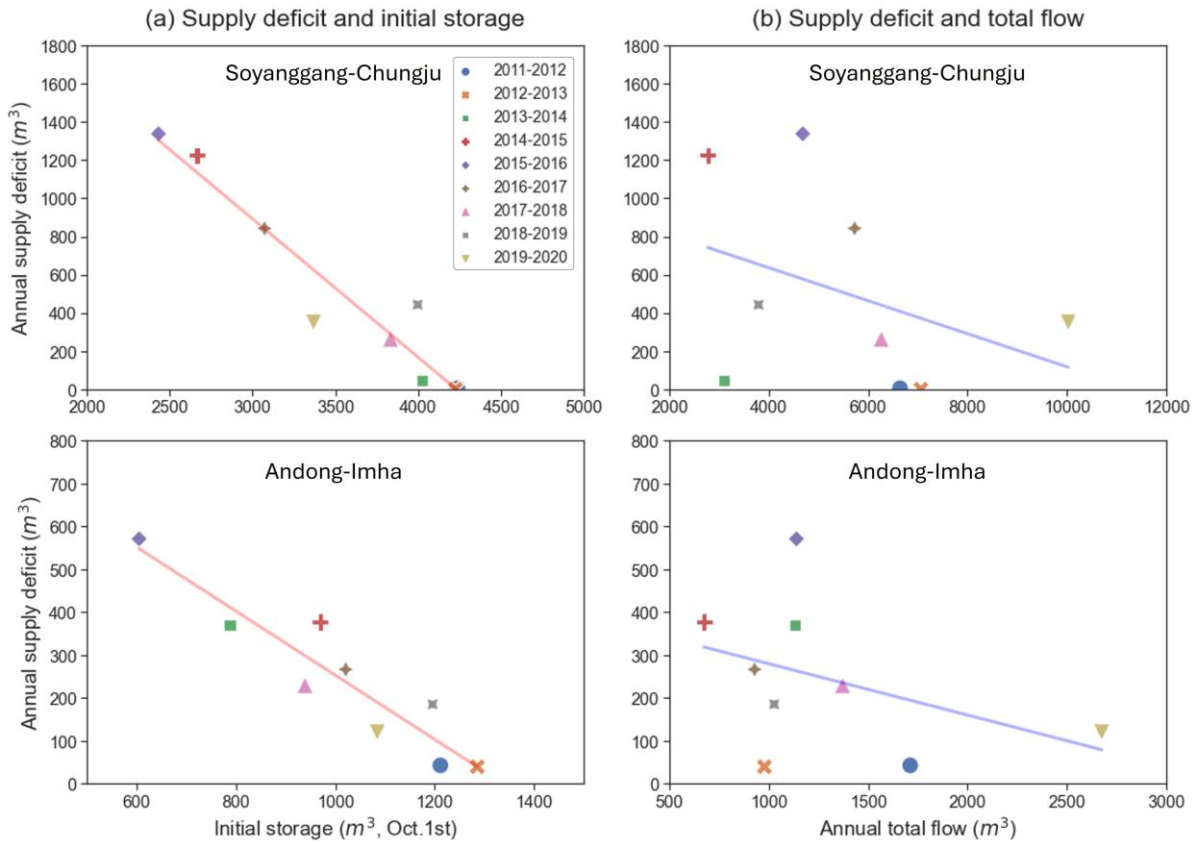

Figure S5: Historical relationship between annual supply deficit (y-axis) and (a) initial storage at the beginning of new hydrological year (October 1st) or (b) annual total flow into reservoir over a hydrological year from 2011 to 2020. Frist and second rows represent Soyanggang-Chungju and Andong-imha reservoir systems, respectively.

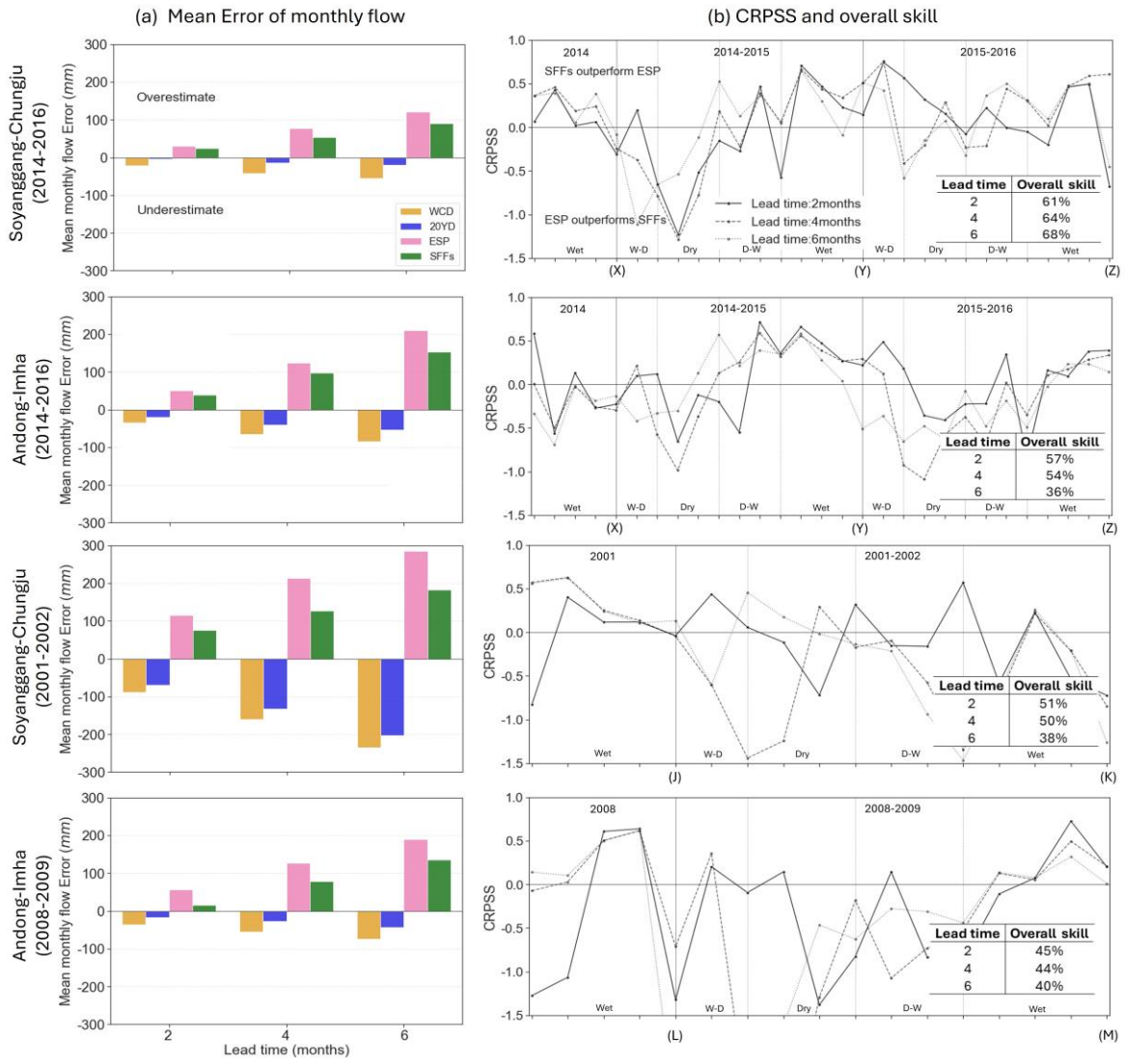

Figure S6: (a) Mean Error of monthly flow (optimised – observed) for 2-month lead time. (b) CRPSS at lead time 2, 4 and 6 months (line plot) and overall skill which represents the frequency of SFFs outperforming ESP (table, bottom right). From top to bottom, the rows represent Soyanggang-Chungju for 2014-2016, Andong-Imha for 2014-2016, Soyanggang-Chungju for 2001-2002 and Andong-Imha for 2008-2009.

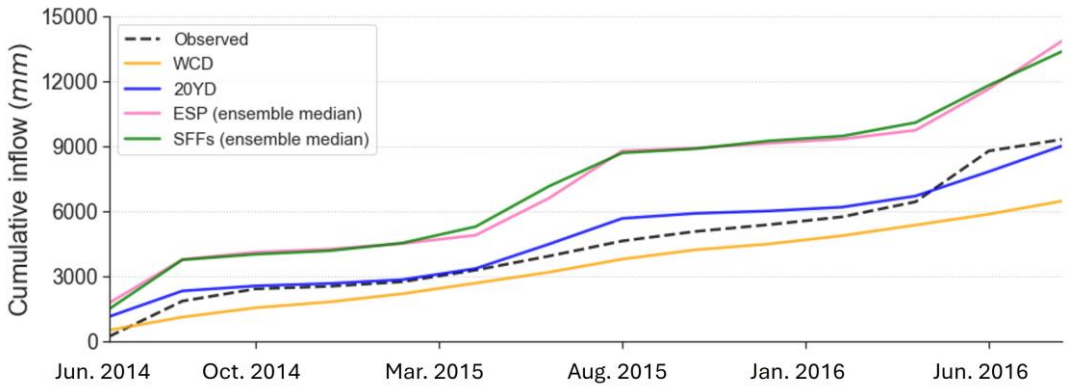

Figure S7: Cumulative flow observation (black dashed line) for Soyanggang-Chungju reservoir system during the 2014-16 drought event, compared to cumulative flows for different flow scenarios/forecasts (all with 2-month lead time).

1. Andong-Imha (2014-2016)

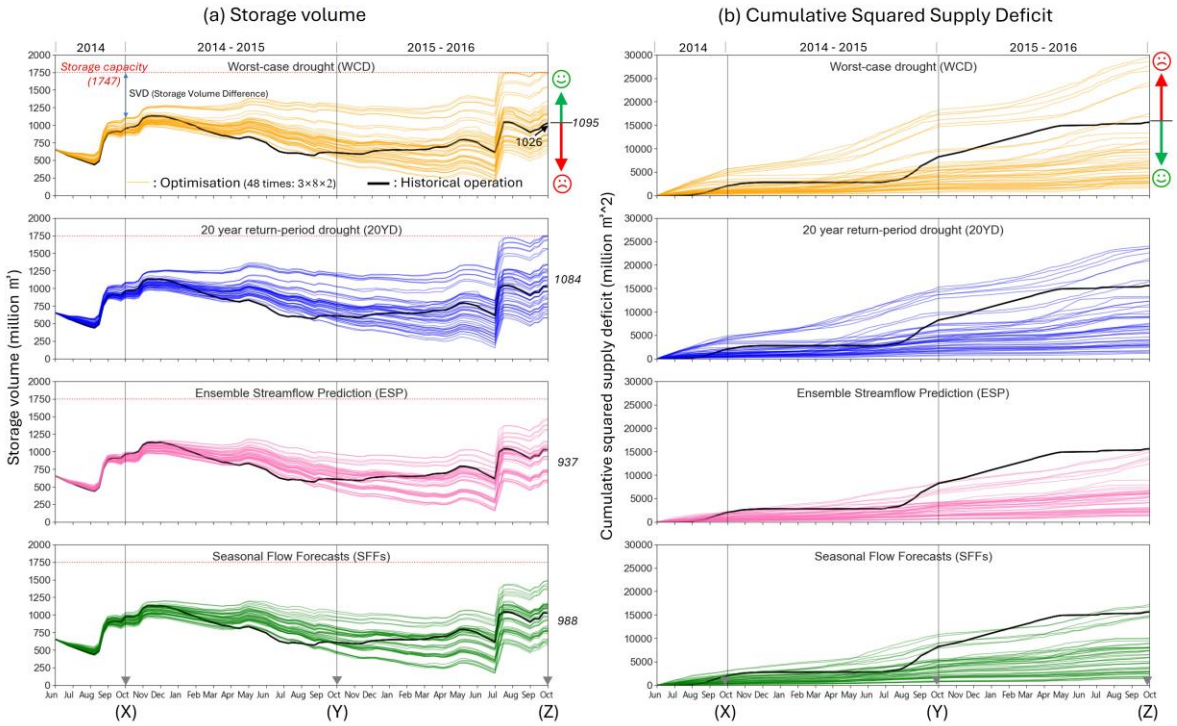

82

2. Soyanggang-Chungju (2001-2002)

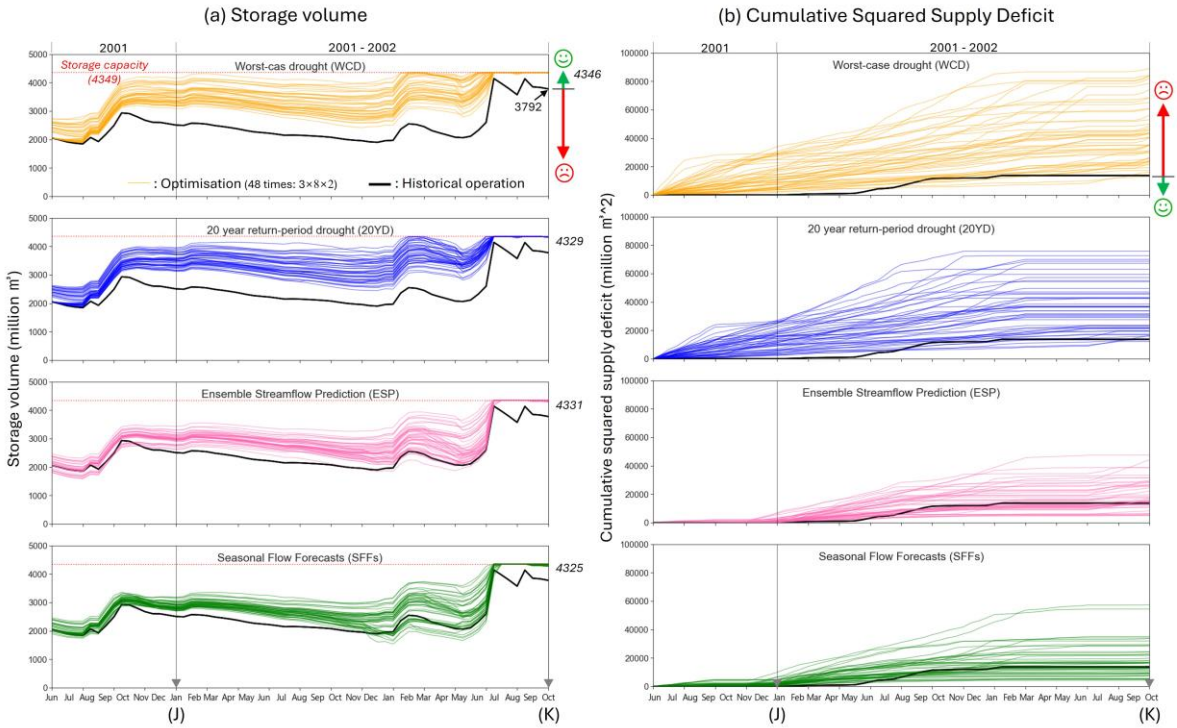

83

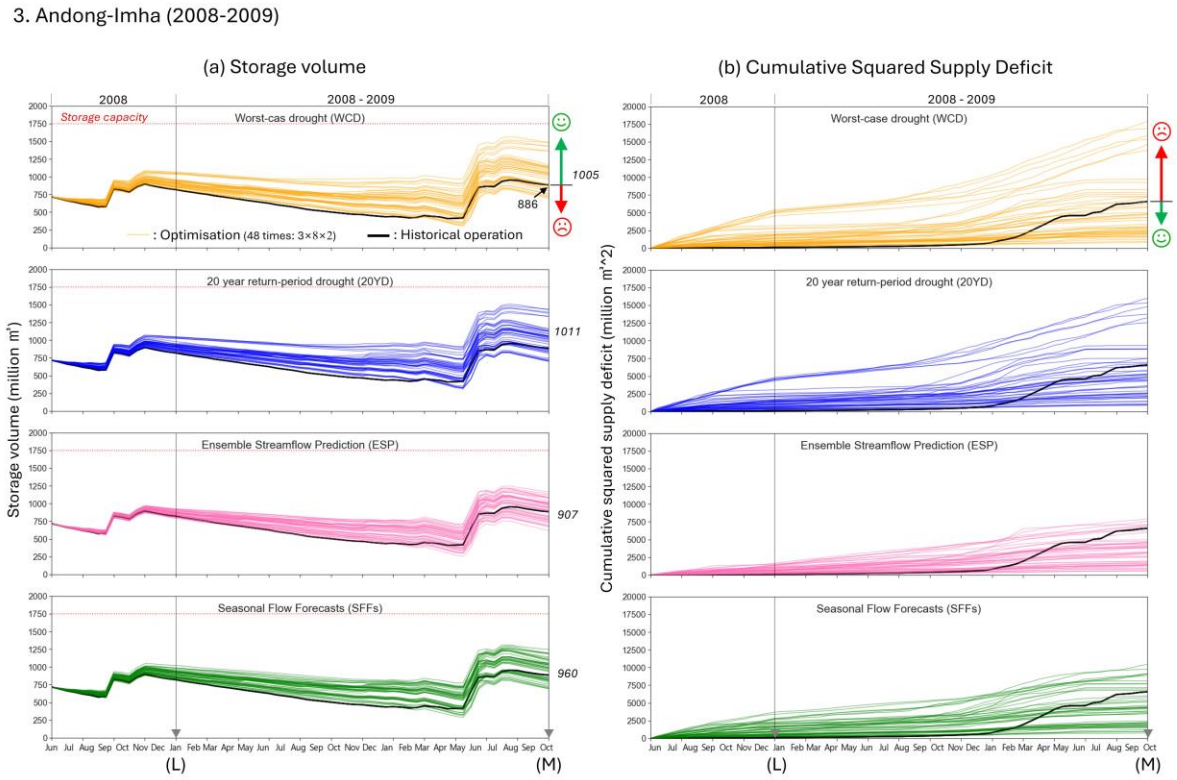

Figure S8: Simulated reservoir operation results for (1) Andong-Imha from June 2014 to September 2016, (2) Soyanggang-Chungju from June 2001 to September 2002 and (3) Andong-Imha from June 2008 to September 2009, in terms of (a) are storage volume and (b) cumulative squared supply deficit. From top to bottom, the rows represent simulation results generated by using WCD (orange), 20YD (blue), ESP (pink), and SFFs (green), respectively. Each sub-figure has 48 simulated results (coloured lines, 3 lead times × 8 MCDM methods × 2 decision-making time steps) and a single historical operation (black line). The numbers indicated at the right end of Figure S8(a) represent the mean storage volume (million m^3) across all 48 simulations.

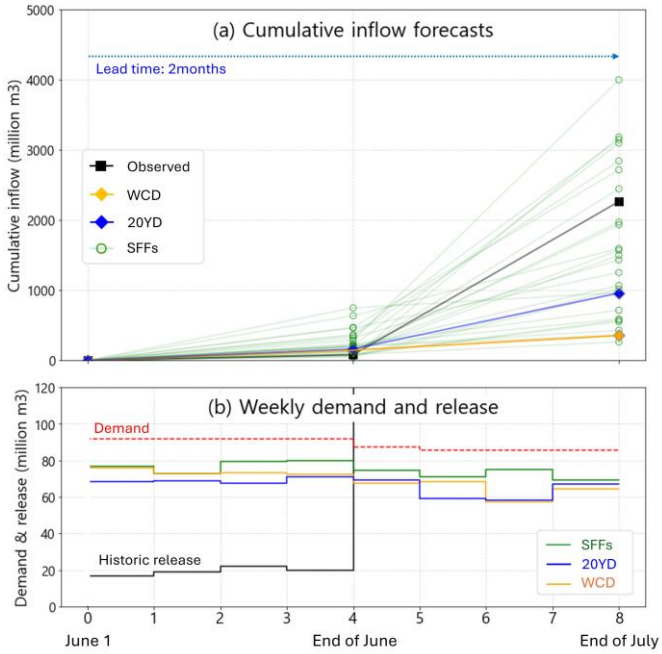

Figure S9: (a) Cumulative flow observation (black square) and forecasts for Soyanggang-Chungju from June to July 2016, using WCD (orange diamond), 20YD (blue diamond), and SFFs (ensemble: hollow green circle, median: red circle). The black square represents the observed cumulative inflow during the same period. (b) Weekly demand (red) and release schedule generated by the multi-objective optimisation fed by the different flow scenarios/forecasts.

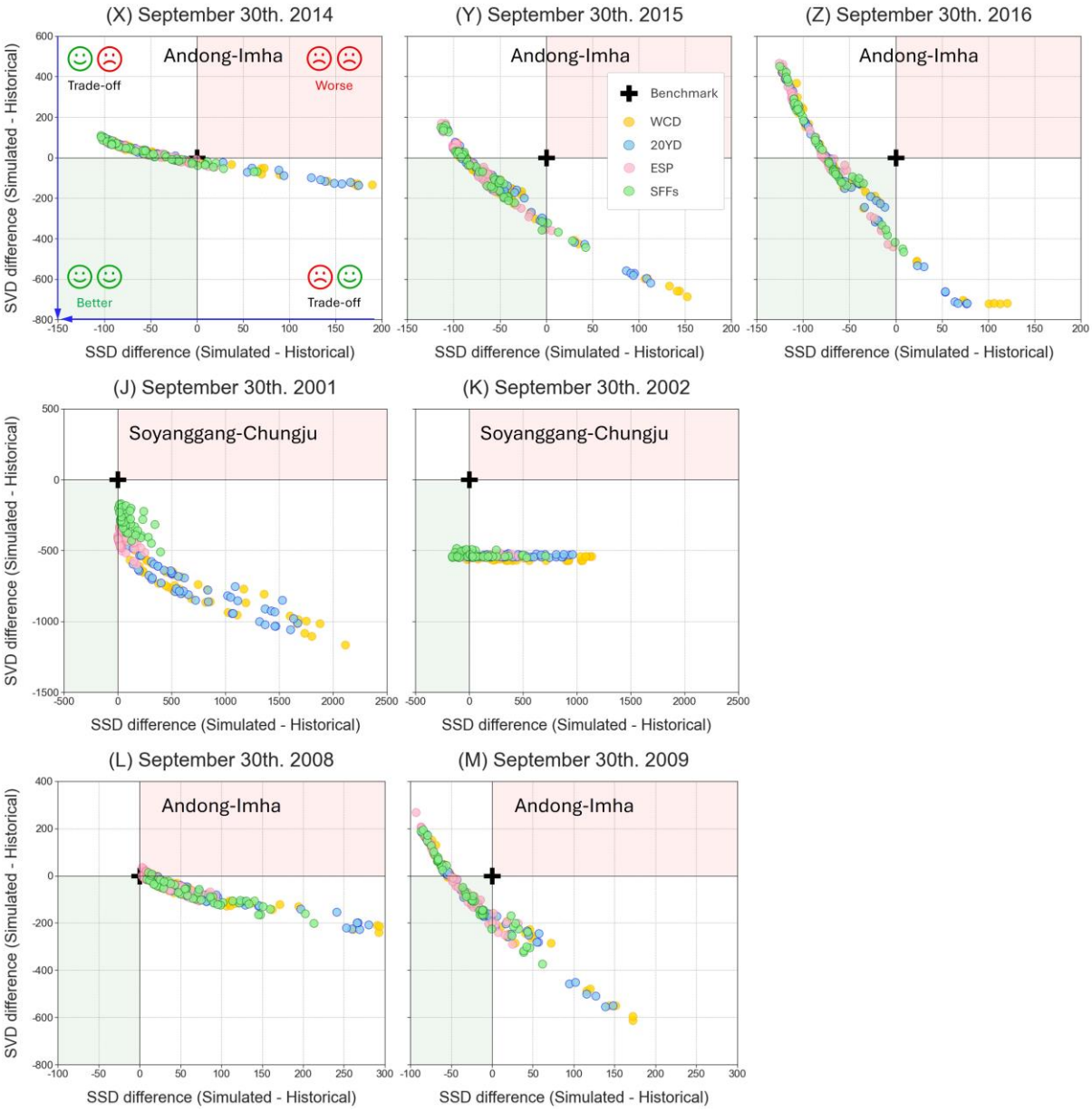

Figure S10: Difference in SSD (x-axis) and SVD (y-axis) between historical operation (black cross) and simulate operations using different flow scenarios/forecasts (coloured circles) in (first row) Andong-Imha during 2014-2016 drought, (second row) Soyanggang-Chungju during 2002-2003 drought and (third row) Andong-Imha during 2008-2009 drought, respectively. Performances are calculated on September 30th in (first row) 2014 (X), 2015 (Y), 2016 (Z) and (second row) 2001 (J), 2002 (K) and (third row) 2008 (L), 2009 (M). Each sub-figure shows 48 points for each flow scenario/forecast (WCD, 20YD, ESP, SFFs), resulting from different combinations of key experimental choices (3 lead times × 8 MCDM methods × 2 decision-making time steps).

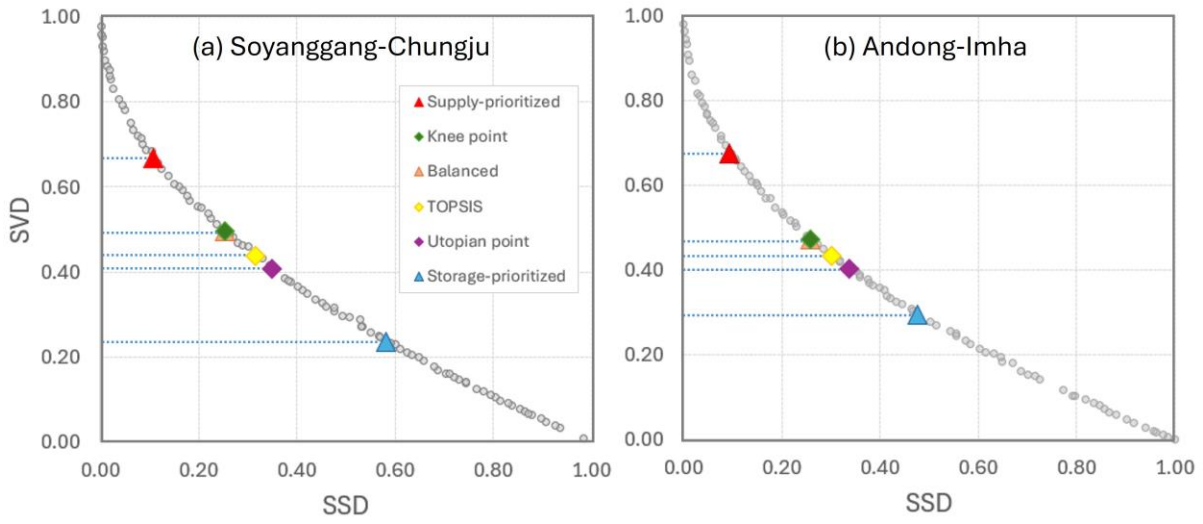

Figure S11: Examples of the Pareto front generated by the reservoir operations optimiser for (a) Soyanggang-Chungju and (b) Andong-Imha in June 2014. A distinct trend can be seen whereby the selected solutions always appear in the same ranking moving from left to right of the horizontal axis: first the Supply-prioritised approach, followed by the Knee point, Balanced, TOPSIS, Utopian point and, finally, the Storage-prioritised approach. The variable weighting methods (Simple Selective, Multi Weighting) do not show such clear pattern and thus are not depicted in this figure for simplicity of e illustration.

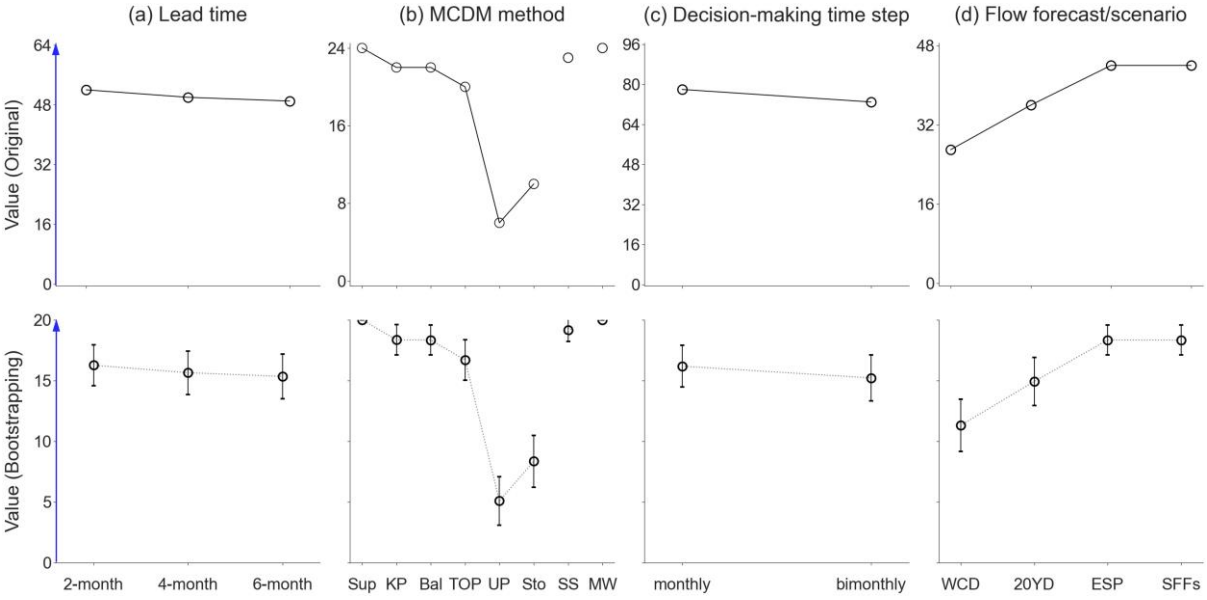

Figure S12: Top row: Forecast value (y-axis) against key experimental choices: (a) forecast lead time, (b) MCDM method, (c) decision-making time step and (d) type of flow forecast/scenario for Soyanggang-Chungju reservoir system on September 30th, 2016. (i.e. Same figure plots as in bottom row of Figure 8). Bottom row: Forecast value generated using 3000 bootstrap resamples, each with a size of 20. The MCDM methods are ordered from left to right with increasing importance to storage availability (see Figure S11), along with two variable weighting methods (SS and MW).

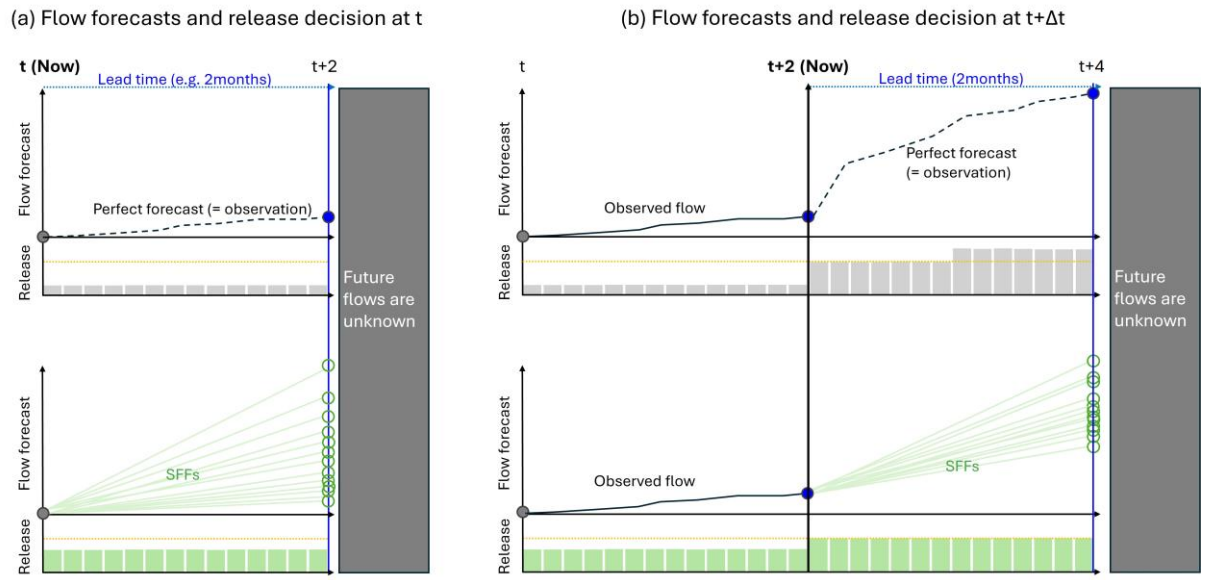

119

120 **Figure S13: Conceptual illustration of the flow forecasts and release decision-making using a perfect forecast (upper**
121 **row) and SFFs (lower row) at time t (a) and t + Δt (b).**

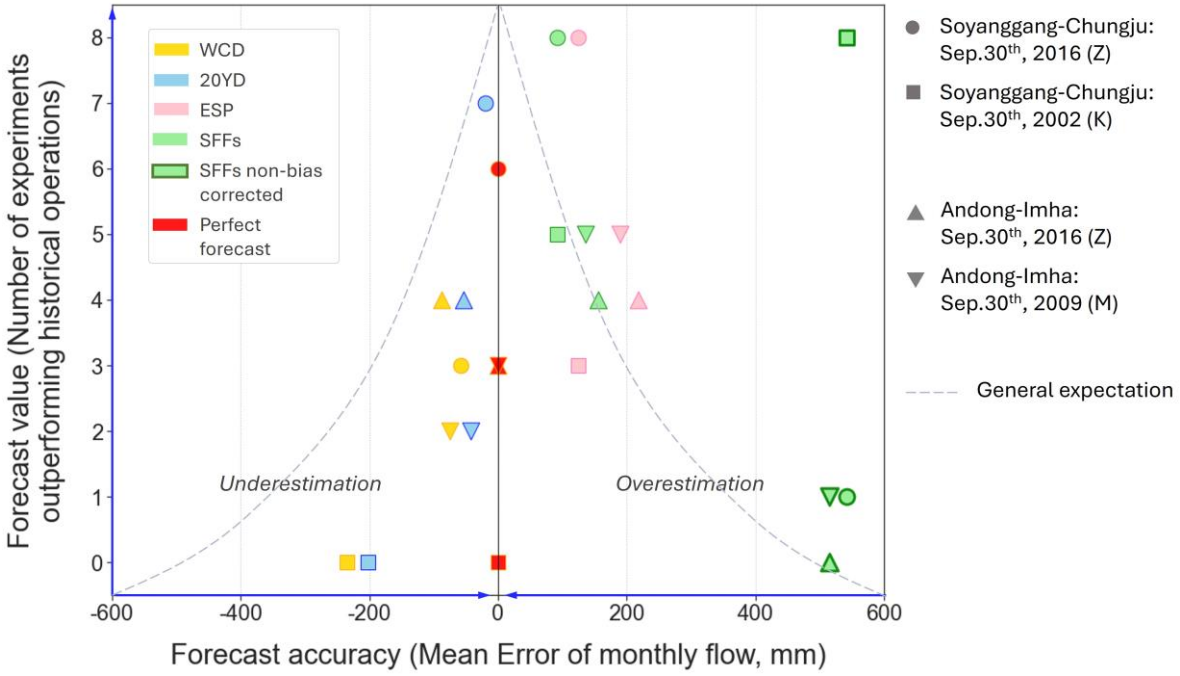

122

123 **Figure S14: Relationship between forecast accuracy (mean error of monthly flow, mm, x-axis) and value tallied over 8**
124 **MCDM methods (number of experiments outperforming historical operations, y-axis) at the end of the simulation**
125 **period for different drought events (2002, 2009 and 2016) at Soyanggang-Chungju and Andong-Imha reservoir**
126 **systems. For each event and system, the figure shows five points corresponding to simulated forecast-informed**
127 **operations using different scenarios/forecasts (orange: WCD, blue: 20YD, pink: ESP, green: SFFs, red: perfect**
128 **forecast). Here, green symbols with (without) outlines represents bias corrected (non-bias corrected) SFFs, respectively.**
129 **The perfect forecast scenario was generated using actual flow observations as future forecasts. The direction of the**
130 **blue arrows indicates higher performance (high value, low error), and the grey dashed lines represent the general**
131 **expectation on the relationship between forecast accuracy and value.**

References

Arsyah, U.I., Jalinus, N., Syahril, Ambiyar, Arsyah, R.H and Pratiwi, M.: Analysis of the Simple Additive Weighting method in educational aid decision making, *Turkish Journal of Computer and Mathematics Education*, 12(14), 2389–2396, https://doi.org/10.17762/turcomat.v12i14.10664, 2021.

Chen, C.-T.: Extensions of the TOPSIS for group decision-making under fuzzy environment, *Fuzzy Sets and Systems*, [online] 114(1), 1–9, https://doi.org/10.1016/s0165-0114(97)00377-1, 2000.

Chiu, W.-Y., Yen, G.G. and Juan, T.-K.: Minimum Manhattan distance approach to multiple criteria decision making in multiobjective optimization problems, *IEEE Transactions on Evolutionary Computation*, 20(6), 972–985, https://doi.org/10.1109/tevc.2016.2564158, 2016.

Das, I.: On characterizing the 'knee' of the Pareto curve based on normal-boundary intersection, *Structural Optimization*, 18(2), 107–115, 1999.

Fishburn, P.C.: Additive utilities with finite sets: Applications in the management sciences, *Naval Research Logistics Quarterly*, 14(1), 1–13, https://doi.org/10.1002/nav.3800140102, 1967.

Han, J. and Kamber, M.: Data mining: concepts and techniques. Amsterdam; Boston: Elsevier/Morgan Kaufmann, 2012.

Hwang, C.L. and Yoon, K.: *Multiple attribute decision making: methods and applications, A state-of-the-art survey*, Springer-Verlag, New York, 1981.

Li, W., Zhang, G., Zhang, T. and Huang, S.: Knee point-guided multiobjective optimization algorithm for microgrid dynamic energy management, *Complexity*, 2020, 1–11, https://doi.org/10.1155/2020/8877008, 2020.

Liu, P.: Multi-attribute decision-making method research based on interval vague set and TOPSIS method, *Technological and Economic Development of Economy*, 15(3), 453–463, https://doi.org/10.3846/1392-8619.2009.15.453-463, 2009.

Lu, L. anderson-Cook, C.M. and Robinson, T.J.: Optimization of designed experiments based on multiple criteria utilizing a Pareto frontier, *Technometrics*, 53(4), 353–365, https://doi.org/10.1198/tech.2011.10087, 2011.

Marler, R.T. and Arora, J.S.: Survey of multi-objective optimization methods for engineering. *Structural and Multidisciplinary Optimization*, [online] 26(6), 369–395, https://doi.org/10.1007/s00158-003-0368-6, 2004.

Mathew, M., Sahu. S. and Upadhyay. A.: Effect of normalization techniques in robot selection using weighted aggregated sum product assessment, *International Journal of Innovative Research and Advanced Studies*, 4(2), 59–63, 2017.

Tzeng, G.H and Huang, J.: *Multiple attribute decision making: methods and applications*, Boca Raton (Florida): Crc Press, 2011.

Vafaei, N., Ribeiro, R.A. and Camarinha-Matos, L.M.: Assessing Normalization Techniques for Simple Additive Weighting Method, *Procedia Computer Science*, 199, 1229–1236, https://doi.org/10.1016/j.procs.2022.01.156, 2022.

Wang, Z. and Rangaiah, G.P.: Application and analysis of methods for selecting an optimal solution from the Pareto-optimal front obtained by multiobjective optimization, *Industrial & Engineering Chemistry Research*, 56(2), 560–574, https://doi.org/10.1021/acs.iecr.6b03453, 2017.

Zhu, F., Zhong, P., Xu, B., Wu, Y. and Zhang, Y.: A multi-criteria decision-making model dealing with correlation among criteria for reservoir flood control operation, *Journal of Hydroinformatics*, 18(3), 531–543, https://doi.org/10.2166/hydro.2015.055, 2015.